# Sex Differences in Kidney Function and Metabolism Assessed Using Hyperpolarized [1-$^{13}$C]Pyruvate Interleaved Spectroscopy and Nonspecific Imaging

Yibo Wen[1,2], Haiyun Qi[1], Christian Østergaard Mariager[1], Per Mose Nielsen[1], Lotte Bonde Bertelsen[1], Hans Stødkilde-Jørgensen[1], and Christoffer Laustsen[1]

[1]MR Research Centre, Department of Clinical Medicine, Aarhus University, Aarhus, Denmark; and [2]The First Affiliated Hospital of Zhengzhou University, Zhengzhou University, Henan, China

**Corresponding Author:**
Christoffer Laustsen, PhD
The MR Research Centre, Department of Clinical Medicine, Aarhus University, Aarhus University Hospital, Palle Juul Jensens Boulevard 99, 8200 Aarhus N, Denmark;
E-mail: cl@clin.au.dk

**Key Words:** MRI, sex, kidney, renal metabolism, hyperpolarization, BSSFP, spectroscopy

**Abbreviations:** Blood oxygenation level-dependent (BOLD), dynamic contrast-enhanced (DCE), magnetic resonance imaging (MRI), fatty acid (FA), magnetic resonance spectroscopy (MRS), magnetic resonance spectroscopic imaging (MRSI), dynamic nuclear polarization (DNP), dissolution dynamic nuclear polarization (dDNP), free induction decay (FID), balanced steady-state free precession (BSSFP), glomerular filtration rate (GFR)

**ABSTRACT**

Metabolic sex differences have recently been shown to be particularly important in tailoring treatment strategies. Sex has a major effect on fat turnover rates and plasma lipid delivery in the body. Differences in kidney structure and transporters between male and female animals have been found. Here we investigated sex-specific renal pyruvate metabolic flux and whole-kidney functional status in age-matched healthy Wistar rats. Blood oxygenation level–dependent and dynamic contrast-enhanced (DCE) magnetic resonance imaging (MRI) were used to assess functional status. Hyperpolarized [1-$^{13}$C]pyruvate was used to assess the metabolic differences between male and female rats. Female rats had a 41% ± 3% and 41% ± 5% lower absolute body and kidney weight, respectively, than age-matched male rats. No difference was seen between age-matched male and female rats in the kidney-to-body weight ratio. A 56% ± 11% lower lactate production per mL/100 mL/min was found in female rats than in age-matched male rats measured by hyperpolarized magnetic resonance and DCE MRI. Female rats had a 33% ± 11% higher glomerular filtration rate than age-matched male rats measured by DCE MRI. A similar renal oxygen tension (T2*) was found between age-matched male and female rats as shown by blood oxygenation level–dependent MRI. The results were largely independent of the pyruvate volume and the difference in body weight. This study shows an existing metabolic difference between kidneys in age-matched male and female rats, which indicates that sex differences need to be considered when performing animal experiments.

## INTRODUCTION

Metabolic sex differences are gaining increasing attention as an important factor in tailoring treatment strategies. Men are at an increased risk of developing nondiabetic renal disease compared to age-matched women (1). Type-2 diabetic women have a greater risk of renal dysfunction than type-2 diabetic men, potentially resulting from an increased susceptibility to poor metabolic control (2). Furthermore, women typically have considerably more body fat, higher whole-body fat turnover rates, and higher plasma triglycerides than men (3). Recent reports have shown sex-specific myocardial metabolic patterns, suggesting differences in treatment effects among male and female

individuals. Divergent responses to metformin in myocardial fatty acid (FA) metabolism between women and men appear to explain the lack of treatment effects when treatment groups were analyzed as a whole (4, 5). It is likely, that similar renal metabolic and functional differences exist between men and women. The existence of sex differences could play an important role in designing and interpreting preclinical and clinical experiments. An increasing number of experimental studies indicate that there are in fact sex differences in both renal rodent models and in human subjects (6–9). Moreover, the differences of renal transporters and renal ammonia metabolism have been reported in rodents with fundamental structural difference between males

and females ([10], [11]). Thus, caution in the translation of the results between sexes is imperative. Previous reports have shown morphological differences between male and female rats of >50% for epithelial volume and absolute volume of proximal tubule ([12]). However, sex difference in renal pyruvate metabolism has, to the best of our knowledge, not been previously reported. The development of hyperpolarized $^{13}$C magnetic resonance spectroscopy (MRS) and spectroscopic imaging (MRSI) based on dissolution dynamic nuclear polarization (dDNP) has enabled unprecedented noninvasive visualization of normal and abnormal metabolism in living systems, without the use of ionizing radiation ([13]–[15]). This novel method relies on the ability to trace the metabolic conversions of intravenously injected molecules, such as hyperpolarized $^{13}$C-pyruvate, as it undergoes metabolic conversion into its metabolic derivatives: $^{13}$C-lactate, $^{13}$C-alanine, and $^{13}$CO$_2$/$^{13}$C-bicarbonate ([16]–[19]). Here we investigated the potential for monitoring the functional and metabolic signatures of age-matched (8 weeks) female and male rats, which received the same volume of hyperpolarized [1-$^{13}$C]pyruvate. To investigate the dose-related impact of pyruvate, an additional group of dose-matched male rats (5 weeks) was included. Dynamic contrast-enhanced (DCE) MRI in combination with hyperpolarized [1-$^{13}$C]pyruvate MRI was performed on both age-matched male and female rats. The combination of perfusion and metabolic conversion, that is, fractional perfusion, allowed us to account for the substrate delivery ([20]), which could be different between males and females. This metric can be simplified by using the hyperpolarized tracer itself, and thus, we investigated if a simple combination of 2 standard sequences could be used as surrogates for the more elaborate imaging sequences typically used. A new interleaved imaging and spectroscopy approach (Figure 1) was used. The sequence consists of a standard slice selective fully balanced steady-state free precession (BSSFP) sequence interleaved with a slice-selective free induction decay (FID) spectroscopic sequence. This would allow high temporal–spatial localization of hemodynamics and the spectroscopic information with high spectral resolution and as such represent a good compromise for many examinations. The rationale for the proposed method is that as the first pass-perfusion is largely dominated by the substrate signal ([21], [22]), the metabolic conversion is dominated by kidney metabolism ([23]), thus offering an alternative approach to image the functional and metabolic features of the kidneys.

## METHODS

### Animal Model

Male (8 week old; $343.9 \pm 6$ grams; n = 8) and female (8 week old; $203.7 \pm 7$ grams; n = 8) Wistar rats were included in this study. The age-matched male and female rats received the same volume of hyperpolarized [1-$^{13}$C]pyruvate, that is, 1 mL. In addition, 8 male Wistar rats (5 week old; $183.2 \pm 3$ grams) exposed to similar experimental conditions was compared to the age-matched male and female rats to test if the dose of the pyruvate injection influences the results. The dose-matched male rats received a hyperpolarized [1-$^{13}$C]pyruvate volume similar to the female rats, that is, 4.9 mL/kg. The details on the rats and the dose of received pyruvate are listed in Table 1. The rats were kept in standard rodent cages with 12/12 h light/dark cycle,

temperature of $21 \pm 2°$C, and humidity of $55\% \pm 5\%$. All rats had free access to water and standard rat chow throughout the study. The experiment started after 1 week of acclimatization. All procedures regarding this experiment complied with the guidelines for use and care of laboratory animals. The study was approved by the Danish Inspectorate of Animal Experiments. The rats were anesthetized with 2.5% sevoflurane in 2 L/min of air. A tail vein catheter (0.4 mm) was inserted for injection of both hyperpolarized [1-$^{13}$C]pyruvate, which was polarized in a 5-T SPINLab (GE Healthcare, Brondby, Denmark) as previously described ([24]). A MRI contrast agent (Dotarem; Guerbet, Roissy, France) was used for DCE measurements. Respiration, body temperature, and peripheral oxygen saturation were monitored during the experiment as previously described ([24]).

Magnetic resonance (MR) scanning procedures were performed using a 9.4-T preclinical MR system (Agilent, Yarnton, UK) with VnmrJ 4.0A (Agilent, Santa Clara, CA), using a dual-tuned $^{13}$C/$^1$H volume rat coil (Doty Scientific, Columbia, SC) as previously described ([25], [26]). The MR data were reconstructed and analyzed using MATLAB (MathWorks, Natick, MA) and Osirix ([27]). The kidney parenchyma regions of interest (ROIs) were manually drawn.

### Hyperpolarized MR

Anatomical $^1$H MRI scans were conducted to determine the location of the kidneys. Afterwards, hyperpolarized [1-$^{13}$C]pyruvate MR imaging and spectroscopy was performed to quantify renal hemodynamics and metabolic conversion of [1-$^{13}$C]pyruvate, respectively. A balanced steady-state free precession (BSSFP) imaging sequence was interleaved with a standard slice-selective free induction decay (FID) acquisition to acquire spectra, both sequences using the same slice selection parameters (see online supplemental Figure 1 and Figure 1). Parameters for the BSSFP sequence were: 1 echo, repetition time (TR) = 2.2 milliseconds, echo time (TE) = 1.1 milliseconds, matrix = $32 \times 32$, field of view (FOV) = $60 \times 60$ mm$^2$, flip angle = 30°, and slice thickness = 15 mm, with a total scan time of 70 milliseconds. Parameters for the FID acquisition were: TR = 206 milliseconds, flip angle = 15°, spectral width = 10 000 Hz, and complex points = 2048. A delay was inserted before each acquisition, to fix the TR to 2 seconds. This was chosen to allow renewal of the hyperpolarized [1-$^{13}$C] pyruvate magnetization pool in the imaging slice. Nineteen images from BSSFP imaging, used for perfusion analysis, and 19 spectra from FID acquisition, used to acquire the metabolites data, were acquired. Age-matched rats received a bolus of 1 mL (125 mM) of hyperpolarized [1-$^{13}$C]pyruvate. The other 8 male rats received hyperpolarized [1-$^{13}$C]pyruvate according their body weight, matching the dose per weight that female rats received, that is, 4.9 mL/kg (612.5 μmol/kg). The interleaved acquisition was initiated at the beginning of the injection. The spectra were analyzed in MATLAB for metabolic information, using an in-house general linear model fitting of the known peaks similar to that mentioned in the literature ([28]). The areas under curve (AUCs) of spectral peaks of [1-$^{13}$C]pyruvate and its metabolic products were calculated for the total signal. The DCE images were analyzed using the Osirix software. The cortex of kidneys was drawn manually to calculate kidney hemodynamics in the Osirix UMMPerfusion plugin ([29]). A T1 relaxation time of
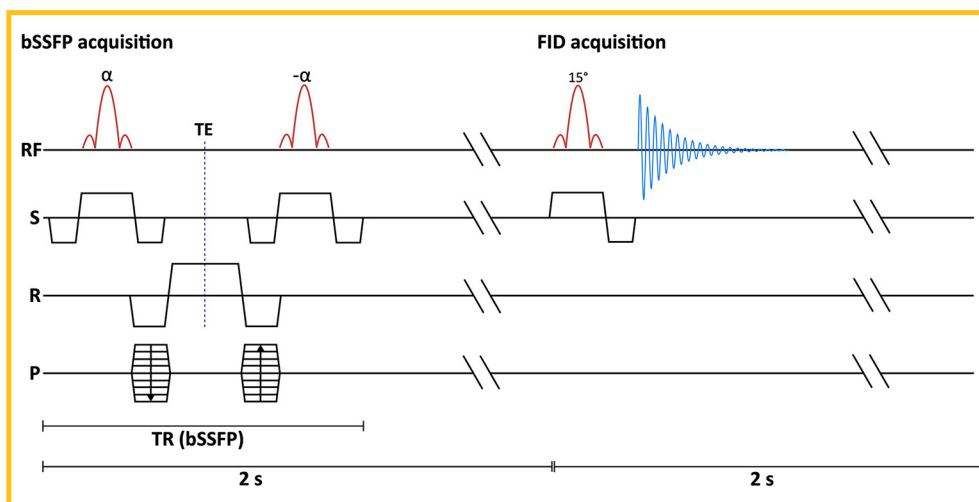
**Figure 1.** Illustration of the interleaved sequence protocol, using a standard 2D slice-selective balanced steady-state free precession (BSSFP) sequence interleaved by a slice-selective free inductive decay spectroscopic sequence. For simplicity in the experimental setup, a 2-second time resolution was used for each acquisition.

20 seconds was used for pyruvate T1 correction of the perfusion data (21, 30). Fractional perfusion, used to correct the metabolic information for the pyruvate delivery, was calculated by multiplying the metabolic ratios with the DCE-derived perfusion (20).

### BOLD MRI

Blood oxygen level–dependent (BOLD) MRI was performed (Figure 2) to measure the oxygen tension in the kidneys of the male and female rats. A standard multiecho gradient echo sequence with 10 echoes was used to acquire 5 slices; TR = 118 milliseconds, TE = 2.0 milliseconds, $\Delta$TE = 2.2 milliseconds, FOV = $70 \times 70$ mm$^2$, matrix = $128 \times 128$, flip angle = 30°, and slice thickness = 1 mm. T2* maps were fitted as previously described and evaluated using the modified 6-layer concentric objects method for ROI analysis (31, 32).

### DCE MRI

DCE MRI (Figure 1) was performed using a gradient echo sequence with the following parameters: TR = 13.7 milliseconds, TE = 1.9 milliseconds, FOV = $60 \times 60$ mm$^2$, matrix = $128 \times 128$, flip angle = 15°, and slice thickness = 20 mm. Acquisition was initiated 10 seconds before administration of MRI contrast to acquire a baseline, with a time resolution of 1.75 seconds in 180 time steps. A single 1-mL bolus isotonic saline containing 0.05 mL of Gadoteric acid (Dotarem; 279.3 mg/mL; Guerbet, Villepinte, France) was administered over 10 seconds. Kidney hemodynamics (Perfusion, MTT, and blood volume) were calculated in the Osirix UMMPerfusion plugin as previously described

(29). Glomerular filtration rate (GFR) was estimated using the Baumann–Rudin model as previously described (33).

### Tissue Harvesting

After the MR examination, $\sim$5 mL of arterial blood was collected from the aortic bifurcation from each anesthetized rat before sacrifice. Further, 1 mL of arterial blood was used for ABL blood–gas analysis. The remaining 4 mL of blood was centrifuged for 10 minutes at 1500 g to separate the plasma which was stored in a −80°C freezer for further analysis. The renal cortex and inner medulla were also stored at −80°C.

### Quantitative Polymerase Chain Reaction (QPCR)

The fresh frozen cortex tissue was used to measure the messenger RNA (mRNA) of monocarboxylate transporter (MCT) 1-4, pyruvate dehydrogenase (PDH), alanine aminotransferase (ALT), and lactate dehydrogenase (LDH) (see online supplemental Table 1). In brief, total RNA was isolated using NucleoSpin RNA II mini kit according to the manufacturer's instructions (AH Diagnostics, Aarhus, Denmark). RNA was quantified by spectrophotometry and stored at −80°C. cDNA synthesis was performed with RevertAid First Strand cDNA synthesis kit (MBI Fermentas, Burlington, Canada). QPCR was performed using Maxima SYBR Green qPCR Master Mix according to the manufacturer's instructions (AH Diagnostics). In brief, 100 ng of cDNA was used as template for PCR amplification. Specificity of products was confirmed by melting curve analysis and by gel electrophoresis.

### Statistics

All data are presented as mean $\pm$ SEM. All statistical analysis was performed in GraphPad Prism 6 (GraphPad Software, Inc. La Jolla, CA). Normal distribution was tested by a Shapiro–Wilk normality test and QQ-plots. Data were analyzed using either an unpaired 2-tailed Student $t$ test or a 2-way-ANOVA with repeated measures; multiple comparisons was corrected using a Tukey correction when appropriate. A value of $P < .05$ was considered statistically significant.
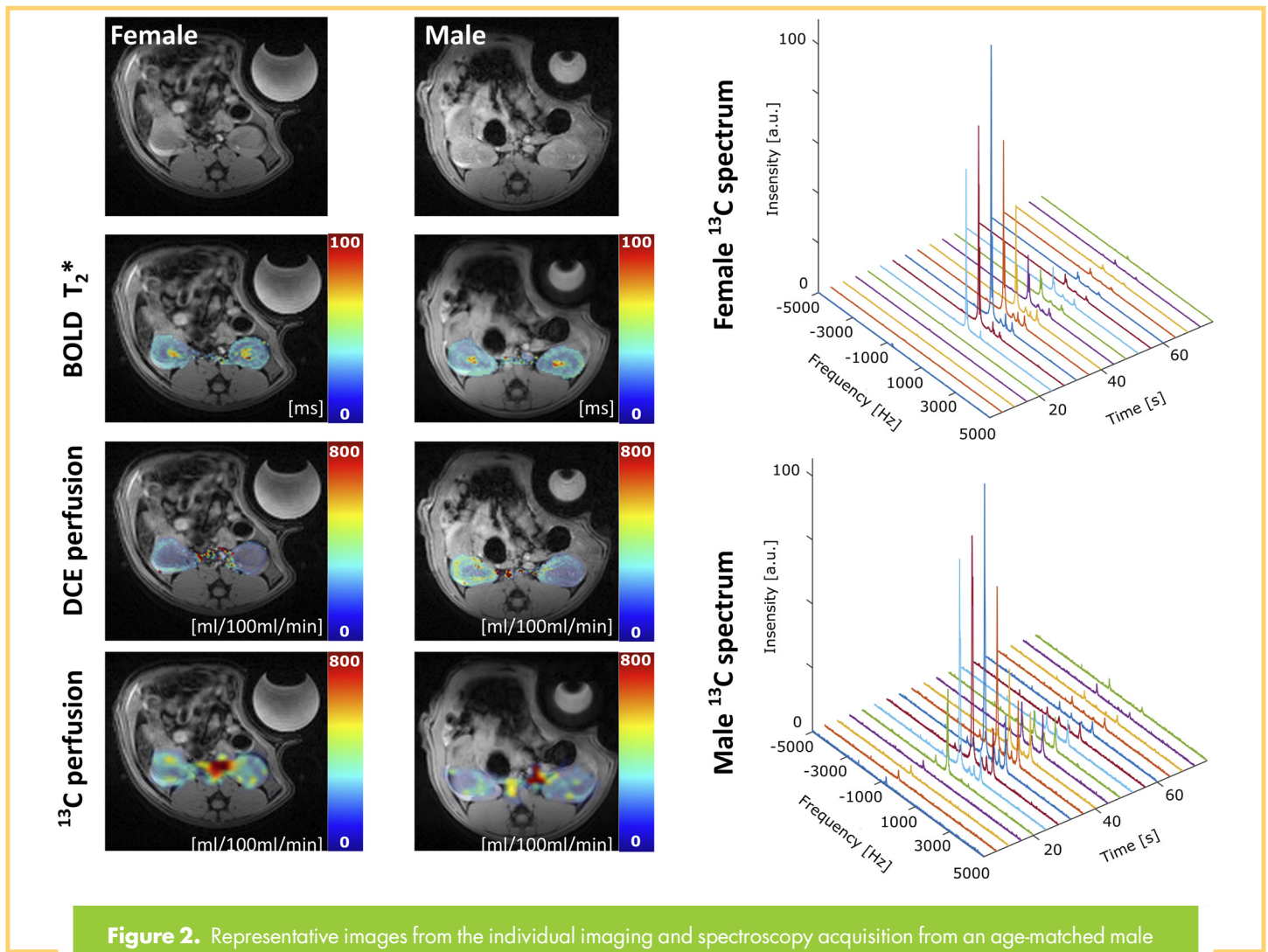
**Table 1.** Age, Body Weight and Received Volume of Hyperpolarized Pyruvate

| Rats Groups | Body Weight (g) | Received Volume (mL) |
|---|---|---|
| 8-week-old female | 203.7 ± 7.2 | 1.0 |
| 8-week-old male | 343.9 ± 6.0 | 1.0 |
| 5-week-old male rats | 183.2 ± 3 | ≈1.2 (4.9 mL/kg) |

**Figure 2.** Representative images from the individual imaging and spectroscopy acquisition from an age-matched male and a female rat.

## RESULTS

### Sex Differences in Anatomy and Blood

A statistically significant difference was observed between age-matched male and female rats, in body weight (BW) and kidney weight (KW), albeit the kidney weight was similar if correction for body weight was performed (Table 2). All data in online supplemental Table 2 was found to be similar between age-matched male and female rats, except for the arterial potassium level (lower in the female rats) and the blood hematocrit and hemoglobin (increased in female rats), which showed an insignificant difference (see online supplemental Table 2).

### Sex Differences in Renal Function

A numerical increased renal plasma flow and mean transit time was found in the male rats, but the difference was not statistically significant (Figure 3, A and C). However, a statistically significant lower renal blood volume ($P = .034$) was found in female rats than in age-matched male rats (Figure 3B). Interestingly, an increased GFR was found in female rats than in male rats (Figure

**Table 2.** Body Weight (BW), Kidney Weight (KW, Mean of Both Kidney's), Blood Glucose Level (Fed State) at the Day of the Scan and Kidney Weight Per Kilogram Rat (KW/BW)

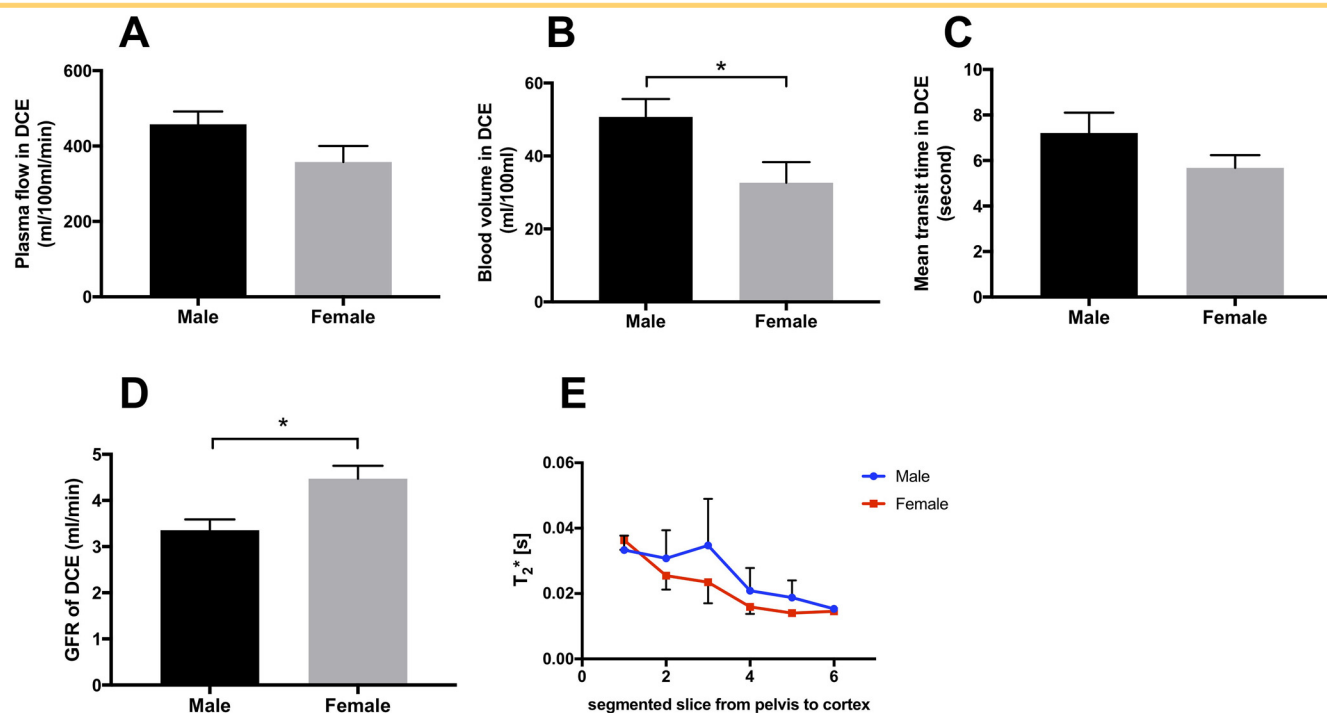|  | Body Weight (g) | Kidney Weight (g) | KW/BW (g/kg) | Blood Glucose Level (mmol/L) |
|---|---|---|---|---|
| 8-week-old male | 343.90 ± 6.00 | 1.16 ± 0.03 | 3.36 ± 0.08 | 7.64 ± 0.27 |
| 8-week-old female | 203.70 ± 7.21* | 0.70± 0.03* | 3.44 ± 0.12 | 7.00 ± 0.42 |

*$P < .05$ versus male group.

**Figure 3.** Renal hemodynamic features in age-matched male and female rats. A similar plasma flow was observed between male and female rats ($P = .095$) (A). A lower renal blood volume of 35.6% was observed in female rats than in male rats ($P = .034$) (B). A similar, although insignificant, mean transit time was observed in male and female rats ($P = .16$) (C). A 32.8% increase in glomerular filtration rate (GFR) was observed in female rats than in male rats ($P = .01$) (D). A similar decreased $^1H$ $T_2^*$ relaxation (surrogate for oxygen availability) from cortex to pelvis was observed in both male and female rats (E). Data are illustrated as means $\pm$ SEM. $*P < .05$ versus male group.

3D) ($P = .009$). A similar renal oxygen tension was found between age-matched male and female rats, both demonstrating a significant increased oxygen tension (decreased $^1H$ $T_2^*$ values) from pelvis to cortex (Figure 3E) ($P < .0001$).

**Differences in Renal Metabolism Related to Sex**
Age-matched male and female rats showed different sex-dependent metabolic responses as measured with $[1-^{13}C]$pyruvate (Figure 4A; $P = .002$). Male rats had a higher lactate/pyruvate ratio than female rats ($P < .0001$), while alanine/pyruvate and bicarbonate/pyruvate did not show a significant difference. When normalized to kidney weight, the 3 metabolites showed no significant difference between the 2 groups (Figure 5A). A significant difference in the perfusion of metabolites was found between the 2 sexes (Figure 4B, $P = .0002$), mainly in the higher fractional perfusion of lactate in the male group than in the female group ($P < .0001$). The fractional perfusion of alanine and bicarbonate was not significantly different. When normalized to kidney weight, the fractional perfusion of the 3 metabolites showed a similar tendency but without significant difference (Figure 5B). The metabolic balance of the 3 metabolites showed significant differences in the different sex (Figure 4C, $P = .034$). Female rats had higher alanine/lactate ratio than male rats ($P < .0001$), while the aerobic/anaerobic metabolism (bicarbonate/lactate ratio) did not show significant difference between age-matched male and

female groups. When comparing the fraction of different metabolites in the total $^{13}C$ metabolite signal($\Sigma$ $^{13}C$-metabolites), a higher lactate/$\Sigma$ $^{13}C$-metabolites ratio ($P = .0018$) and a lower alanine/$\Sigma$ $^{13}C$-metabolites ratio ($P = .0003$) was found in male rats than in female rats, and there were no significant differences in the bicarbonate/$\Sigma$ $^{13}C$-metabolites ratio (Figure 4D) between age-matched male and female rats. No correlation was seen between $^1H$ DCE and $^{13}C$-perfusion assessment using a nonselective BSSFP ($P = .20$, $R^2 = 0.13$). Expression levels of pyruvate metabolic related enzymes of LDH, PDH, ALT, and MCT1-4 did not reveal any sex-specific differences, although a numerical tendency was observed (see online supplemental Figure 1). To test if the constant dose used for the pyruvate injection had an effect on the metabolic profile, another 8 male rats (5 week old) received the matched dose of hyperpolarized $[1-^{13}C]$pyruvate injection that was given to the female rats (Table 1). Interestingly, the fractional lactate production was increased in male dose-matched rats (Figure 5C) than in female rats. Inspecting the pyruvate normalized metabolic distribution (Figure 5D) in the different groups, a similar tendency was observed with an increased lactate production, while the alanine production was less pronounced. To verify the body weight or age dependence on the metabolic difference between male and female rats, a correlation analysis was performed on the lactate production in the male rats with different body weights (spanning the female rat
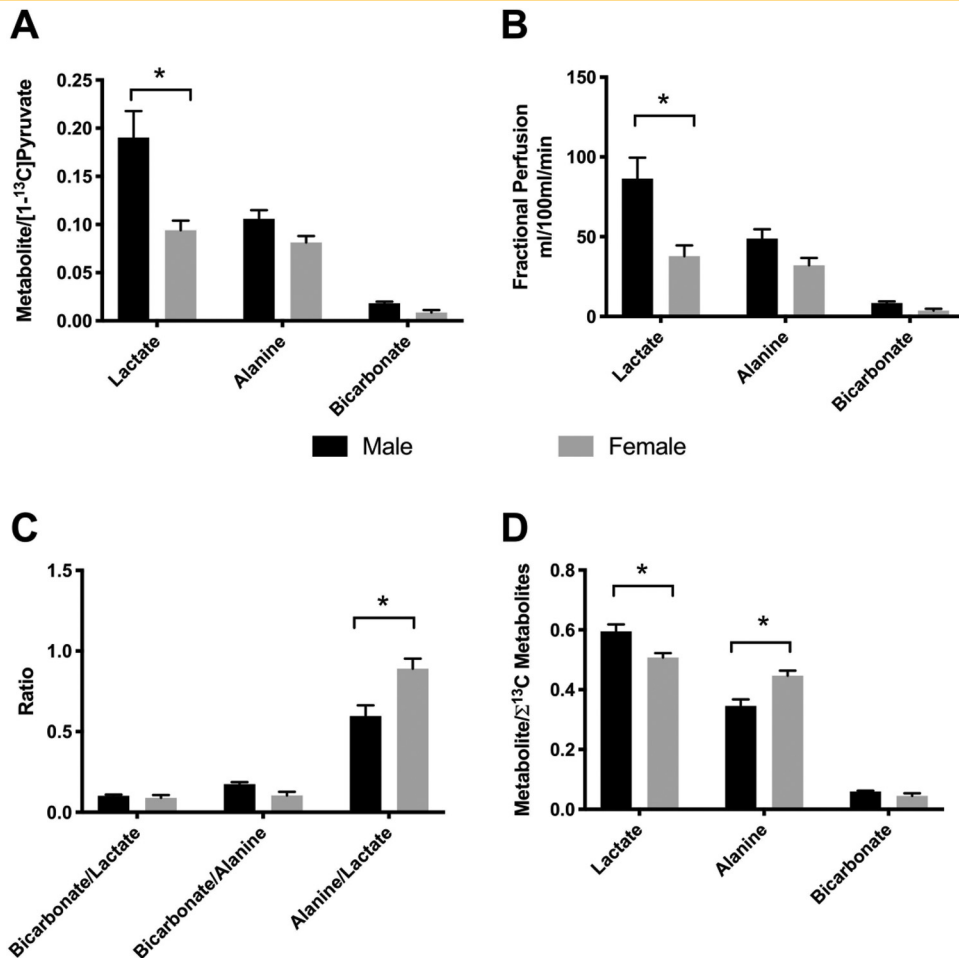
**Figure 4.** Renal metabolic features in age-matched male and female rats. The aerobic and anaerobic metabolic response in male and female rats measured using $^{13}$C pyruvate. Different metabolite-to-pyruvate ratios, where female rats had 50.6% lower lactate/pyruvate ratio than male rats ($P < .0001$), while the alanine/pyruvate ratio ($P = .46$) and bicarbonate/pyruvate ratio ($P = .94$) did not show any significant differences between the male and female rats (A). Correcting the metabolic conversion for renal perfusion (fractional perfusion), did not alleviate the metabolic difference between the male and female kidneys. Female rats had 56.3% lower fractional perfusion of lactate than male rats ($P < .0001$), without significantly different fractional perfusion of alanine ($P = .24$) or bicarbonate ($P = .945$) (B). The metabolic product balance of the 3 metabolites: lactate, alanine and bicarbonate, similarly showed a shift in balance between amino-acids and lactate in male rats. It showed a 49.4% lower alanine/lactate ratio ($P < .0001$) than in female rats, albeit no difference was found for the balance between bicarbonate and lactate ($P = .996$), as well as bicarbonate and alanine ($P = .51$) (C). A 14.7% higher lactate fraction ($P = .0018$) and 29.4% lower alanine fraction ($P = .0003$) in male rats, while a similar bicarbonate fraction ($P = .91$), was found in the fraction of the metabolic products lactate, alanine, and bicarbonate (D). Data are illustrated as means $\pm$ SEM. *$P < .05$ versus male group.

body weights). No significant correlation was observed under these conditions (Figure 5E).

## DISCUSSION

The main finding of this study was the significant differences in renal function and associated metabolic profile between the female and male groups, showing a generally elevated metabolic activity in male kidneys. The mRNA expression levels of pyruvate metabolic-related enzymes of LDH, PDH, ALT, and MCT1-4 did not reveal significant sex-specific differences. One potential reason for this metabolic difference could be the number of nephrons, which previously has been correlated with kidney size (34, 35). This is supported by the higher body weight and kidney weight levels found in the male group than in the female group, while the kidney-weight to body-weight ratio shows no significant difference between the groups. This suggest that kidney growth is well matched with body weight. However, correction for the metabolic conversion by kidney weight reduced the metabolic differences, which indicates that the number of nephrons
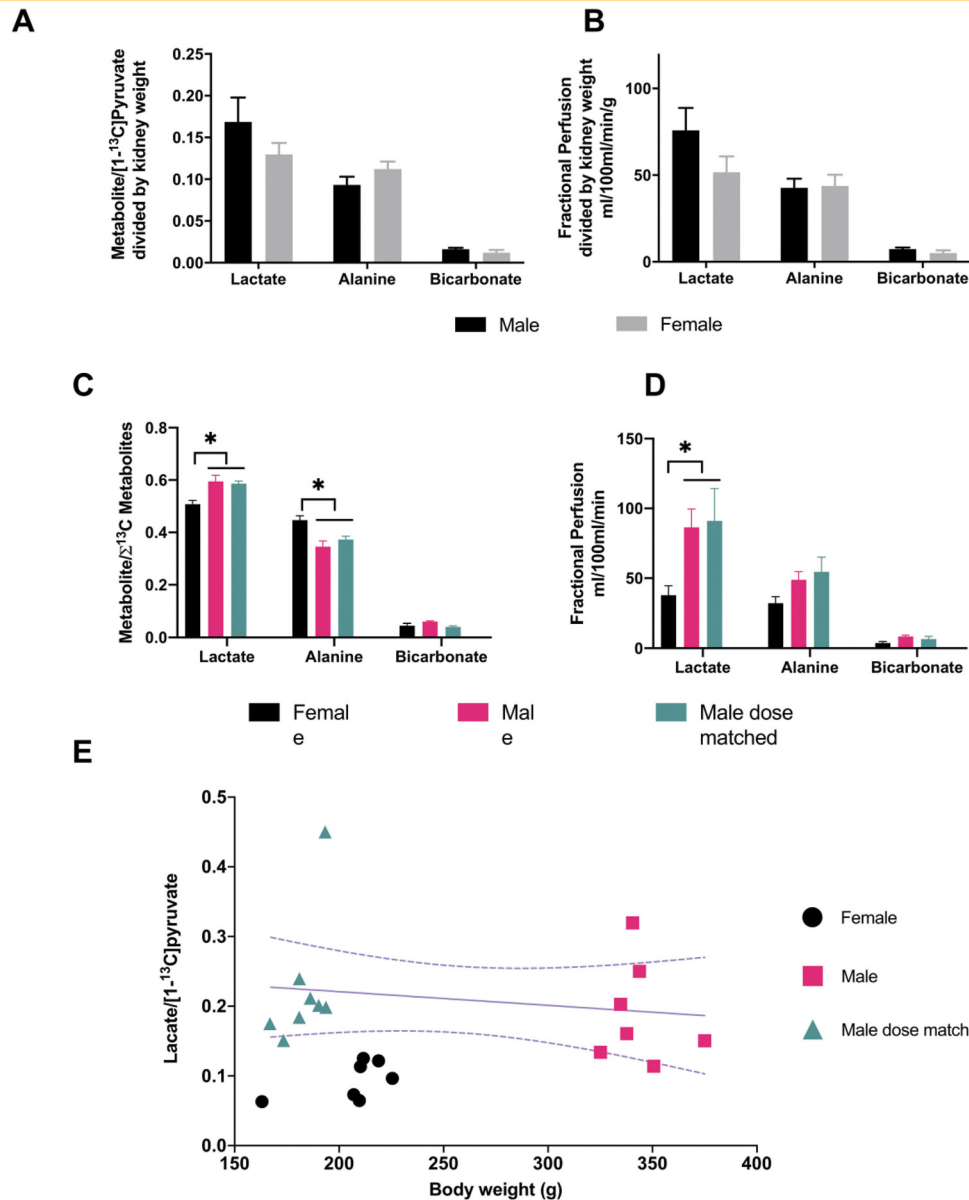
**Figure 5.** Comparison between age-matched male and female rats as well as dose-matched rats. Illustrates different metabolite/pyruvate ratio normalized by kidney weight, where there is no significant difference between male rats and female rats (sex $P = .50$, interaction term sex × metabolites $P = .14$, metabolites $P < .0001$) (A). By correcting with the kidney weight, a similar tendency was seen (increased lactate fractional perfusion in males compared with females), but did not show significant difference (sex $P = .17$, interaction term sex × metabolites $P = .19$, metabolites $P < .0001$) (B). A significant difference was found between female and male rats ($P = .0076$) and female and dose-matched male rats ($P = .0023$), in the fractional perfusion of lactate, while no differences were seen in alanine and bicarbonate perfusion (sex, $P = .0077$, interaction term sex × metabolites $P = .17$, metabolites $P < .0001$) (C). A distinct metabolic distribution was seen between the female and male rats in the pyruvate normalized case (sex $P > .99$; interaction term sex × metabolites $P < .0001$, metabolites $P < .0001$) (D). Linear regression showed no significant correlation of lactate production and body weight in male rats ($P = .32$), while the female rats has a significantly lower lactate production compared to males (E).

could be the origin of this sex difference. In humans, females also generally have smaller kidneys with fewer nephrons than males (36, 37). To examine if the metabolic differences could be affected by different body weights and thus the injected dose between age-

matched male and female rats, 1 additional male group with a lower body weight was examined. The injected dose of hyperpolarized [1-$^{13}$C]pyruvate was matched to that of the female rats. The lower-body-weight male rats showed an increase in lactate

production compared to female rats. The differences were less pronounced between the age-matched males and dose-matched males and thus support sex differences as an important parameter in designing and interpreting preclinical results. We speculate that this could be similar in humans, as female patients with diabetes are often at a higher risk of renal dysfunction than males (38), as well as the fact that renal protection has been associated with an increased metabolic activity (39). The acquisition strategy was found to have a less pronounced effect, although it was found to impact the metabolic pools and as such represents an important point when comparing preclinical data even among same-sex individuals. Recent publications using hyperpolarized $^{13}$C magnetic resonance imaging suggest that this technique may enable simultaneous measurement of renal metabolism and perfusion (22), even with nonselective imaging if the metabolic conversion is low enough (21). However, the use of a nonmetabolic imaging approach, here a standard BSSFP, did not correlate well with the DCE perfusion. This is likely owing to the large contribution from the metabolites, and thus, a more spectral selective approach is needed in situations with high metabolic conversion. These findings together support the translation of hyperpolarized MR to human examinations, using more selective imaging methods. The fundamental metabolic information observed in this study can help improve patient stratification, by addressing metabolic sex differences. The major limitation to this study is the fact that the female cycle was not considered (10, 11), which could potentially impact the metabolic status even further. We first compared the age-matched males and females with an equal volume of pyruvate injected. However, owing to the large bodyweight difference between age-matched males and females, a group of dose-matched younger male rats was added, which received a pyruvate

volume matching the dose per body weight that female rats received. Regardless, both aged-matched and dose-matched males showed similar increased conversion of pyruvate to lactate compared with the female rats, which indicated that metabolic sex differences are larger than body weight differences, and comparing values between studies among same sex was reasonable. It is important to keep in mind that the injected concentrations are many times higher than the supraphysiological concentrations used in human studies and therefore unlikely a substrate-limited regime (40). The injected pyruvate concentration can have an influence on the conversion rate of pyruvate to lactate; however, as illustrated in Table 1, a small difference of 10%–20% of the injected dose is unlikely main contributor to the overall significant metabolic difference between male and female rats. The injected concentration of pyruvate (612.5 µmol/kg) is well above the saturation limit for in vivo experiments (41). This is supported by the fact that no correlation was seen between the male groups and the lactate production. Furthermore, a very similar metabolic profile between the 2 male groups, despite significantly different body weights, was seen. Together these data call for further studies to fully elucidate the impact on growth and sex patterns and in particular opens the possibility for hyperpolarized MR to aid in the development of sex-tailored treatments of renal diseases. It is however clear from this study that it is important to consider sex in the comparison of hyperpolarized data, as the metabolic phenotype can be different between males and females.

## Supplemental Materials

Figure 1: https://doi.org/10.18383/j.tom.2020.00022.sup.01
Table 1: https://doi.org/10.18383/j.tom.2020.00022.sup.02
Table 2: https://doi.org/10.18383/j.tom.2020.00022.sup.03

## REFERENCES

1. Neugarten J, Golestaneh L. Gender and the prevalence and progression of renal disease. Adv Chronic Kidney Dis. 2013;20:390–395.
2. Kajiwara A, Kita A, Saruwatari J, Miyazaki H, Kawata Y, Morita K, Oniki K, Yoshida A, Jinnouchi H, Nakagawa K. Sex differences in the renal function decline of patients with type 2 diabetes. J Diabetes Res. 2016;2016:4626382.
3. Mittendorfer B, Magkos F, Fabbrini E, Mohammed BS, Klein S. Relationship between body fat mass and free fatty acid kinetics in men and women. Obesity (Silver Spring). 2009;17:1872–1877.
4. Lyons MR, Peterson LR, McGill JB, Herrero P, Coggan AR, Saeed IM, Recklein C, Schechtman KB, Gropler RJ. Impact of sex on the heart's metabolic and functional responses to diabetic therapies. Am J Physiol Heart Circ Physiol. 2013;305:H1584–1591.
5. Clotet S, Riera M, Pascual J, Soler MJ. RAS and sex differences in diabetic nephropathy. Am J Physiol Renal Physiol. 2016 ajprenal 00292 02015.
6. Zimmerman MA, Baban B, Tipton AJ, O'Connor PM, Sullivan JC. Chronic ANG II infusion induces sex-specific increases in renal T cells in Sprague–Dawley rats. Am J Physiol Renal Physiol. 2015;308:F706–712.
7. Lima-Posada I, Portas-Cortés C, Pérez-Villalva R, Fontana F, Rodríguez-Romo R, Prieto R, Sánchez-Navarro A, Rodríguez-González GL, Gamba G, Zambrano E, Bobadilla NA. Gender differences in the acute kidney injury to chronic kidney disease transition. Sci Rep. 2017;7:12270.
8. Maric C. Sex, diabetes and the kidney. Am J Physiol Renal Physiol. 2009;296:F680–688.
9. Neugarten J, Acharya A, Silbiger SR. Effect of gender on the progression of nondiabetic renal disease: a meta-analysis. J Am Soc Nephrol. 2000;11:319–329.
10. Harris AN, Lee HW, Osis G, Fang L, Webster KL, Verlander JW, Weiner ID. Differences in renal ammonia metabolism in male and female kidney. Am J Physiol Renal Physiol. 2018;315:F211–F222.
11. Sabolic I, Asif AR, Budach WE, Wanke C, Bahn A, Burckhardt G. Gender differences in kidney function. Pflugers Arch. 2007;455:397–429.
12. Oudar O, Elger M, Bankir L, Ganten D, Ganten U, Kriz W. Differences in rat kidney morphology between males, females and testosterone-treated females. Ren Physiol Biochem. 1991;14:92–102.
13. Nelson SJ, Kurhanewicz J, Vigneron DB, Larson PE, Harzstark AL, Ferrone M, van Criekinge M, Chang JW, Bok R, Park I, Reed G, Carvajal L, Small EJ, Munster P, Weinberg VK, Ardenkjaer-Larsen JH, Chen AP, Hurd RE, Odegardstuen LI, Robb FJ, Tropp J, Murray JA. Metabolic imaging of patients with prostate cancer using hyperpolarized [1-(1)(3)C]pyruvate. Sci Transl Med. 2013;5:198ra108.
14. Cunningham CH, Lau JY, Chen AP, Geraghty BJ, Perks WJ, Roifman I, Wright GA, Connelly KA. Hyperpolarized 13C Metabolic MRI of the human heart: initial experience. Circ Res. 2016;119:1177–1182.
15. Coffey AM, Shchepin RV, Truong ML, Wilkens K, Pham W, Chekmenev EY. Open-source automated parahydrogen hyperpolarizer for molecular imaging using (13)C metabolic contrast agents. Anal Chem. 2016;88:8279–8288.
16. Laustsen C, Nielsen PM, Nørlinger TS, Qi H, Pedersen UK, Bertelsen LB, Østergaard JA, Flyvbjerg A, Ardenkjær-Larsen JH, Palm F, Stødkilde-Jørgensen H. Antioxidant

treatment attenuates lactate production in diabetic nephropathy. Am J Physiol Renal Physiol. 2017;312:F192–F199.[10.1152/ajprenal.00148.2016]

17. Laustsen C, Østergaard JA, Lauritzen MH, Nørregaard R, Bowen S, Søgaard LV, Flyvbjerg A, Pedersen M, Ardenkjaer-Larsen JH. Assessment of early diabetic renal changes with hyperpolarized [1-13C]pyruvate. Diabetes Metab Res Rev. 2013;29:125–129.

18. Nielsen PM, Laustsen C, Bertelsen LB, Qi H, Mikkelsen E, Kristensen MLV, Nørregaard R, Stødkilde-Jørgensen H. In situ lactate dehydrogenase activity: a novel renal cortical imaging biomarker of tubular injury? Am J Physiol Renal Physiol. 2017;312:F465–F473.

19. Laustsen C, Hansen ESS, Kjaergaard U, Bertelsen LB, Ringgaard S, Stødkilde-Jørgensen H. Acute porcine renal metabolic effect of endogastric soft drink administration assessed with hyperpolarized [1-(13C)]pyruvate. Magn Reson Med. 2015;74:558–563.

20. Mariager CO, Lindhardt J, Nielsen PM, Schulte RF, Ringgaard S, Laustsen C. Fractional perfusion: a simple semi-parametric measure for hyperpolarized 13C MR. IEEE Trans Radiat Plasma Med Sci. 2019;3

21. Mikkelsen EFR, Mariager CØ, Nørlinger T, Qi H, Schulte RF, Jakobsen S, Frøkiær J, Pedersen M, Stødkilde-Jørgensen H, Laustsen C. Hyperpolarized [1-(13C)]-acetate renal metabolic clearance rate mapping. Sci Rep. 2017;7:16002.

22. Fuetterer M, Busch J, Traechtler J, Wespi P, Peereboom SM, Sauer M, Lipiski M, Fleischmann T, Cesarovic N, Stoeck CT, Kozerke S. Quantitative myocardial first-pass cardiovascular magnetic resonance perfusion imaging using hyperpolarized [1-13C] pyruvate. J Cardiovasc Magn Reson. 2018;20:73.

23. Laustsen C. Hyperpolarized renal magnetic resonance imaging: potential and pitfalls. Front Physiol. 2016;7:72.

24. Qi H, Nielsen PM, Schroeder M, Bertelsen LB, Palm F, Laustsen C. Acute renal metabolic effect of metformin assessed with hyperpolarised MRI in rats. Diabetologia. 2018;61:445–454.

25. Bertelsen LB, Nielsen PM, Qi H, Nørlinger TS, Zhang X, Stødkilde-Jørgensen H, Laustsen C. Diabetes induced renal urea transport alterations assessed with 3D hyperpolarized (13) C,(15) N-Urea. Magn Reson Med. 2017;77:1650–1655.

26. Qi H, Norlinger TS, Nielsen PM, Bertelsen LB, Mikkelsen E, Xu Y, Stodkilde Jorgensen H, Laustsen C. Early diabetic kidney maintains the corticomedullary urea and sodium gradient. Physiol Rep. 2016;4. pii: e12714.

27. Rosset A, Spadola L, Ratib O. OsiriX: an open-source software for navigating in multi-dimensional DICOM images. J Digit Imaging. 2004;17:205–216.

28. Khegai O, Schulte RF, Janich MA, Menzel MI, Farrell E, Otto AM, Ardenkjaer-Larsen JH, Glaser SJ, Haase A, Schwaiger M, Wiesinger F. Apparent rate constant mapping using hyperpolarized [1-(13C)]pyruvate. NMR Biomed. 2014;27:1256–1265.

29. Zollner FG, Weisser G, Reich M, Kaiser S, Schoenberg SO, Sourbron SP, Schad LR. UMMPerfusion: an open source software tool towards quantitative MRI perfusion analysis in clinical routine. J Digit Imaging. 2013;26:344–352.

30. Lee H, Song JE, Shin J, Joe E, Joo CG, Choi YS, Song HT, Kim DH. High resolution hyperpolarized (13) C MRSI using SPICE at 9.4T. Magn Reson Med. 2018;80.

31. Milani B, Ansaloni A, Sousa-Guimaraes S, Vakilzadeh N, Piskunowicz M, Vogt B, Stuber M, Burnier M, Pruijm M. Reduction of cortical oxygenation in chronic kidney disease: evidence obtained with a new analysis method of blood oxygenation level-dependent magnetic resonance imaging. Nephrol Dial Transplant. 2017;32:2097–2105.

32. Mariager CØ, Nielsen PM, Qi H, Ringgaard S, Laustsen C. Hyperpolarized 13C,15N2-urea T2 relaxation changes in acute kidney injury. Magn Reson Med. 2018;80:696–702.

33. Ostergaard Mariager C, Nielsen PM, Qi H, Schroeder M, Bertelsen LB, Laustsen C. Can hyperpolarized (13)C-urea be used to assess glomerular filtration rate? A retrospective study. Tomography. 2017;3:146–152.

34. Luyckx VA, Shukha K, Brenner BM. Low nephron number and its clinical consequences. Rambam Maimonides Med J. 2011;2:e0061.

35. Murawski IJ, Maina RW, Gupta IR. The relationship between nephron number, kidney size and body weight in two inbred mouse strains. Organogenesis. 2010;6:189–194.

36. Hoy WE, Douglas-Denton RN, Hughson MD, Cass A, Johnson K, Bertram JF. A stereological study of glomerular number and volume: preliminary findings in a multiracial study of kidneys at autopsy. Kidney Int Suppl. 2003(;83):S31–37.

37. McNamara BJ, Diouf B, Hughson MD, Douglas-Denton RN, Hoy WE, Bertram JF. Renal pathology, glomerular number and volume in a West African urban community. Nephrol Dial Transplant. 2008;23:2576–2585.

38. Yu MK, Lyles CR, Bent-Shaw LA, Young BA; Pathways Authors. Risk factor, age and sex differences in chronic kidney disease prevalence in a diabetic cohort: the pathways study. Am J Nephrol. 2012;36:245–251.

39. Qi W, Li Q, Gordin D, King GL. Preservation of renal function in chronic diabetes by enhancing glomerular glucose metabolism. J Mol Med. 2018;96:373–381.

40. Kurhanewicz J, Vigneron DB, Ardenkjaer-Larsen JH, Bankson JA, Brindle K, Cunningham CH, Gallagher FA, Keshari KR, Kjaer A, Laustsen C, Mankoff DA, Merritt ME, Nelson SJ, Pauly JM, Lee P, Ronen S, Tyler DJ, Rajan SS, Spielman DM, Wald L, Zhang X, Malloy CR, Rizi R. Hyperpolarized (13)C MRI: path to clinical translation in oncology. Neoplasia. 2019;21:1–16.

41. Zierhut ML, Yen YF, Chen AP, Bok R, Albers MJ, Zhang V, Tropp J, Park I, Vigneron DB, Kurhanewicz J, Hurd RE, Nelson SJ. Kinetic modeling of hyperpolarized 13C1-pyruvate metabolism in normal rats and TRAMP mice. J Magn Reson. 2010;202:85–92.